The effect of trapeziometacarpal joint passive stiffness on mechanical loadings of cartilages

Thomas Valerio, Jean-Louis Milan, Benjamin Goislard de Monsabert, Laurent Vigouroux

Journal of Biomechanics 166 (2024) 112042

Contents lists available at ScienceDirect

Journal of Biomechanics

journal homepage: www.elsevier.com/locate/jbiomech

The effect of trapeziometacarpal joint passive stiffness on mechanical loadings of cartilages

Thomas Valerio [a,b,*], Jean-Louis Milan [a,b], Benjamin Goislard de Monsabert [a], Laurent Vigouroux [a]

[a] Aix-Marseille University, CNRS, ISM, Marseille, France
[b] Aix-Marseille University, APHM, CNRS, ISM, St Marguerite Hospital, Institute for Locomotion, Department of Orthopaedics and Traumatology, Marseille, France

ARTICLE INFO

Keywords:
Trapeziometacarpal joint
Stiffness
Contact pressure
Maximum shear strain
Osteoarthritis

ABSTRACT

Hypermobility of the trapeziometacarpal joint is commonly considered to be a potential risk factor for osteoarthritis. Nevertheless, the results remain controversial due to a lack of quantitative validation. The objective of this study was to evaluate the effect of joint laxity on the mechanical loadings of cartilage.

A patient-specific finite element model of trapeziometacarpal joint passive stiffness was developed. The joint passive stiffness was modeled by creating linear springs all around the joint. The linear spring stiffness was determined by using an optimization process to fit force–displacement data measured during laxity tests performed on eight healthy volunteers. The estimated passive stiffness parameters were then included in a full thumb finite element simulation of a pinch grip task driven by muscle forces to evaluate the effect on trapeziometacarpal loading. The correlation between stiffness and the loading of cartilage in terms of joint contact pressure and maximum shear strain was analyzed.

A significant negative correlation was found between the trapeziometacarpal joint passive stiffness and the contact pressure on trapezium cartilage during the simulated pinch grip task.

These results therefore suggest that the hypermobility of the trapeziometacarpal joint could affect the contact pressure on trapezium cartilage and support the existence of an increased risk associated with hypermobility.

1. Introduction

The trapeziometacarpal (TMC) joint is the principal hand joint affected by osteoarthritis (OA) (Cvijetić et al., 2004). OA in the TMC joint leads to functional capacity reduction which could be an important problem for daily life (Miura et al., 2004; Moriatis Wolf et al., 2014). This pathology originates from systemic and genetic factors (Marshall et al., 2018) and/or with the combination of different types of mechanical loading (principal stress, maximum shear strain) endured by cartilage tissues (Buckwalter et al., 2013; Eskelinen et al., 2019; Hashimoto et al., 2009; Mononen et al., 2018; Orozco et al., 2018; Saarakkala et al., 2010; Saarakkala and Julkunen, 2010; Turunen et al., 2013; Yin and Xia, 2014). Because the mechanical factor appears to be one of the predominant factors, biomechanical models are used to explain OA (Sun et al., 2023). Biomechanical models consist in representing the mechanical behavior of the anatomical structures. By solving the mechanical equations from measured or hypothesized functional boundaries, those models estimate the internal mechanical loading of anatomical structures depending on the task. Multi-body rigid (MBR) models are used to estimate the muscle forces and joint reaction forces involved in movements such as the pinch or the power grip tasks (Barry et al., 2018; Goislard de Monsabert et al., 2014). To estimate stresses and strains in anatomic structures, the most advanced finite element (FE) models are based on CT scan or MRI data, enabling both geometrical and material properties to be precisely defined. Muscle forces assessed by an MBR model are then included as boundary conditions for FE models of osteoarticular structures to estimate the specific mechanical loading on articular cartilage (Dong et al., 2023; Faudot et al., 2020a). This modeling approach provided new insight into OA mechanical risk factors such as the influence of TMC bone morphology or grip types (Valerio et al., 2023). Among the major OA risk factors, previous studies have shown that hypermobility could also be a risk factor for TMC OA development (Jonsson et al., 1996; Jónsson et al., 2009). This assumption could be explained by abnormal loadings due to joint hypermobility

* Corresponding author at: Institute of Movement Science, 163 Avenue de Luminy BP 910 13288, Marseille cedex 09.
E-mail address: handism13@gmail.com (T. Valerio).

https://doi.org/10.1016/j.jbiomech.2024.112042
Accepted 5 March 2024
Available online 6 March 2024

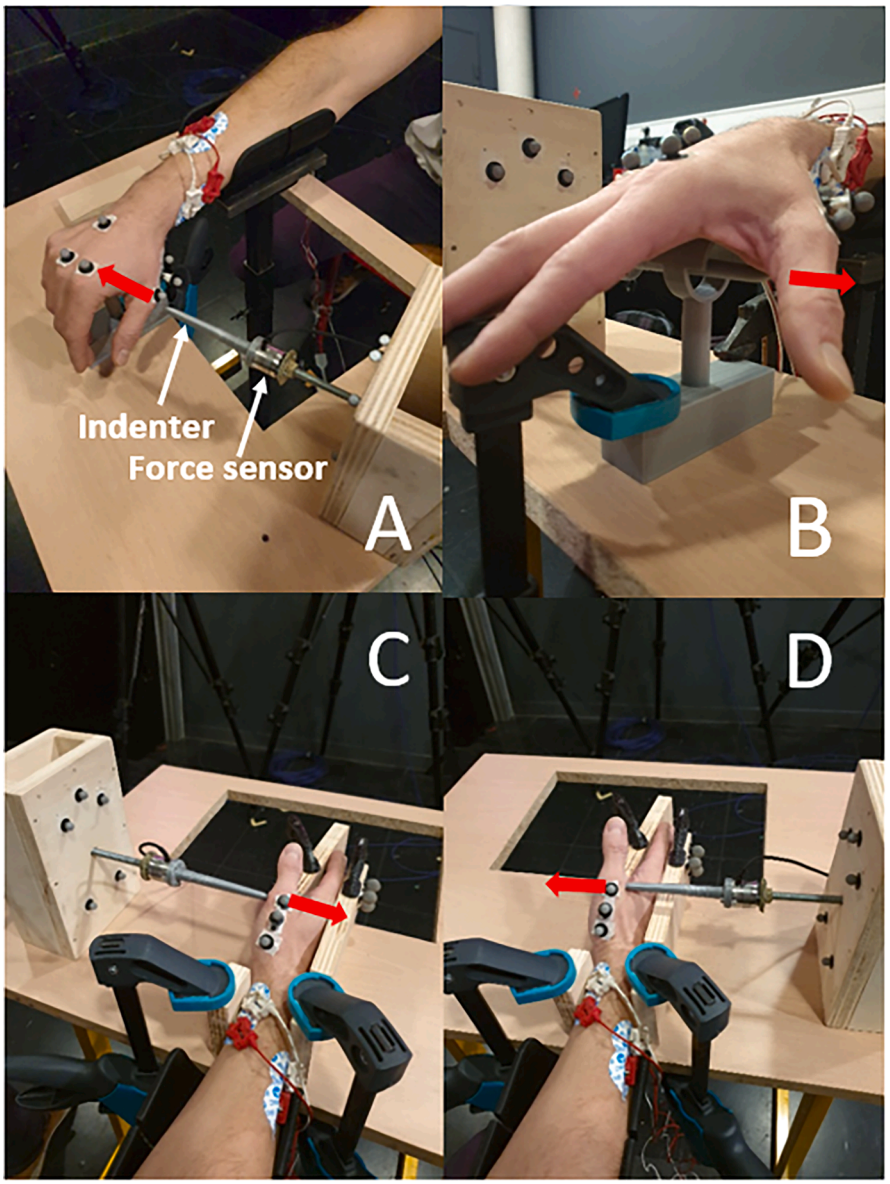

Fig. 1. The experimental system used to measure force–displacement data of the TMC joint during passive movement of flexion (A), extension (B), adduction (C), and abduction (D). The red arrows represent the direction of the force applied by the indenter (3D-printed sharp rod). In the picture, the indenter pushes on the dorsal (A), volar (B), radial (C), and the ulnar (D) side of the first metacarpal head. (For interpretation of the references to colour in this figure legend, the reader is referred to the web version of this article.)

as was observed for the knee joint (Smith et al., 2015). However, for TMC OA, those conclusions are controversial since some other studies have shown no differences in terms of TMC joint mobility between healthy and OA patients (Halilaj et al., 2015). This potential risk factor must therefore be clarified for better understanding and to prevent TMC OA. TMC joint stiffness involves a complex mechanical structure of soft tissue materials, including the ligaments, the muscles, and the joint capsule (Ladd et al., 2012; Norose et al., 2022). Previous studies on ligaments and global stiffness characterization have shown an important interindividual variability in TMC joint stiffness (D'Agostino et al., 2014; Domalain et al., 2010). To clarify the potential effect of hypermobility and to correctly estimate the patient-specific OA risk factor, it appears necessary to consider the specific TMC joint stiffness and its consequences on TMC mechanics. When considering FE models, the joint passive stiffness is classically modeled by taking average values of ligament stiffness from the literature, measured on cadaveric specimens (Bettinger et al., 2000; D'Agostino et al., 2014). Nevertheless, this approach cannot clarify the contribution of individual joint stiffness as a potential risk factor for OA development. Including the patient-specific stiffness in models represents a great challenge because it requires mechanical testing to determine the mechanical properties of the tissues involved in the passive stiffness (Rusli et al., 2021). Previous studies on the knee joint have used an interesting approach to estimate the material properties of ligaments based on in vivo laxity test (Ewing et al., 2016; Kang et al., 2016; Westover et al., 2016). The authors performed several laxity tests during which they recorded the force applied and the bone displacement. They identified the mechanical properties of ligaments using FE models of the knee and an optimization procedure to match experimental force displacement data.

Consequently, to investigate the problem of joint stiffness as a TMC OA risk, the first objective of our present study was to develop a patient-specific estimation of the TMC joint stiffness based on in vivo experimental data, inspired by methodologies performed on the knee. The second objective was to investigate the effect of joint stiffness on mechanical loading of cartilage, by using the patient-specific estimation developed in the first objective. Experimental data were based on laxity

tests whereas force and displacement data were measured on flexion, extension, abduction, and adduction passive movements of the TMC joint, performed on healthy volunteer participants. A computational model of the TMC joint bones was created, based on CT-scan images. Springs were created all around the joint to model the global joint stiffness. A Levenberg-Marquardt optimization method was performed to optimize the spring stiffness of the model to fit experimental data extracted from the laxity tests. Finally, patient-specific models of TMC joint stiffness were used to simulate a pinch grip task and to observe whether, as we hypothesized, TMC joint stiffness is negatively correlated with mechanical loading, represented by principal stress and maximum shear strain in this study.

2. Methods

2.1. Stiffness experimental evaluation

Eight healthy participants (4 men, and 4 women) without previous injury in the hand, aged 20 to 43 years, with first metacarpal length from 4.5 to 5.5 cm, and who signed an informed consent were included in this study. They were seated in front of a table and asked to place their right hand on the table in a neutral position (Fig. 1). Their hands and forearms were placed on a custom splint to be secured during the laxity tests. A custom experimental device was created to perform the laxity tests in passive flexion (Fig. 1a), extension (Fig. 1b), adduction (Fig. 1c), and abduction (Fig. 1d) of the TMC joint. A 3D- printed sharp rod was created with an appropriate size for applying force on the thumb. This experimental system was used to apply force on the dorsal, volar, radial, and ulnar sides of the metacarpal bone head location identified on the participants' skin. Bone tuberosity was identified by palpating the correct area to apply the force. The experimental system allowed the experimenter to manually apply the load on the thumb along a specific axis. For each test, five loading cycles were performed with 2 trials separated by 2 min. During each laxity test, participants were asked to not actively resist the force applied. EMG data were recorded on the flexor pollicis longus (FPL) and the extensor pollicis longus (EPL) muscle to ensure that muscle activity remained negligible. If the normalized root mean square of the EMG signal exceeded 10 %, the trial was canceled. A force sensor (Nano-25, ATI Industrial Automation, Garner, NC) was embedded in the custom experimental device to measure the force applied to the metacarpal head. Thumb movement during laxity tests was measured with a six-camera system (MX T40, Vicon, Oxford, UK). Three skin-mounted markers were placed on the first metacarpal dorsal side and three markers were placed on the hand dorsal side to measure the metacarpal position relative to the hand dorsal side position (Fig. 1). This protocol was approved by the Ethics Committee for Research in Science and Techniques of Physical and Sports Activities (CER STAPS no. IRB00012476-2023-23-03-239).

Local coordinate systems were constructed from the three markers on the metacarpal and hand plane. The cross-product was calculated between the proximo-distal axis (determined by the proximal and distal markers) and the line between the proximal and middle marker to determine the metacarpal radio ulnar axis. The cross-product between the radio-ulnar axis and the proximo-distal axis was finally calculated to determine the metacarpal dorso-volar axis. The same process was performed for the hand plane to determine the dorso-volar, proximo-distal, and radio-ulnar axis of the hand. Orientation of the local coordinate system of the trapezium bone relative to the hand plane was estimated using a rotation matrix with constant angle values (Cooney et al., 1981). Orientation of the local coordinate system on the first metacarpal bone was then calculated relative to the coordinates system of the trapezium bone according to the previous study of (Cheze et al., 2009). In this study, Cheze et al.,)consider the metacarpal bone movement according to the following Euler sequence: flexion–extension, axial rotation, and abduction–adduction. We used the anatomical landmarks from Cheze et al.,)to create the coordinate system on the first metacarpal and trapezium bones to measure the first metacarpal bone displacement numerically. The Euler angles measured were then used in the simulation to align the experiment and simulation. The forces measured in these laxity tests were used as boundary conditions of the FE model, presented in the next part. The Euler angles measured experimentally were used as targets to adjust the TMC joint stiffness in the FE model optimization.

2.2. FE model optimization to identify the subject-specific TMC joint stiffness

A 3D CAD model of the trapezium and the first and second metacarpal bones in the neutral position was created with CT images (slice thickness: 0.625 mm; pixel size: 0.372 mm; resolution: 512 px × 512 px) and segmentation using Mimics (Research 22.0; Materialise, Belgium). The CT images were obtained from one healthy volunteer (male, 43 years), from a previous study of our group (Valerio et al., 2023). One generic bone model was used to isolate the effect of stiffness. This participant was chosen because the curvature values of the first metacarpal and trapezium subchondral bones were the closest to the average values reported in (Valerio et al., 2023) with curvature values of 142.9 mm^{-1}, 70.4 mm^{-1}, 86.2 mm^{-1} and 99.0 mm^{-1} for the trapezium and metacarpal bones dorso-volar and ulno-radial curvatures respectively. The bone surfaces were meshed with triangles (average edge size of 1.3 mm) on 3-Matic (Research 14.0; Materialise, Belgium). The bone surface meshes were converted into volume meshes with tetrahedral elements by using FEBioStudio (Maas et al., 2012). Cartilage was extracted from the subchondral bone surface (manually selected) as prismatic elements with an average thickness of 0.7 mm (Dourthe et al., 2019). Mesh quality metrics for cartilage were checked with a Jacobian higher than 0.4 for 98 % of elements, an aspect ratio under 3 for 96 % of elements, and an angle asymmetry higher than 0.5 for 95 % of elements. Bones were modeled as rigid bodies. Cartilage was modeled as neo-Hookean ($E = 10$ MPa, $\nu = 0.4$) (Dong et al., 2023; Kempson, 1972; Schneider et al., 2017). Since the 4 prismatic layers yielded the same pressure results, 3 layers were considered sufficiently accurate for the cartilage. The cartilage internal surface was tied to the subchondral bone. Contact between the trapezium and metacarpal cartilages was modeled with a sliding elastic contact implemented with a penalty-type method (Dong et al., 2023; Maas et al., 2012; Zimmerman and Ateshian, 2018). The penalty factor was set as 2 with the "auto penalty option" and without the augmented Lagrangian. The trapezium surface was considered as the primary surface.

The stiffness was modeled with nine linear springs located all around the joint to represent stiffness induced by ligaments and the other tissues. Primary simulations showed that nine was the minimum number of springs required to ensure model stability and prevent secondary rotation during the simulations. The springs used were modeled using a phenomenological approach to represent the global TMC joint stiffness that potentially results from all the surrounding tissues and not only from the ligaments of the joint. The force measured in the stiffness experimental evaluation (see previous part) was applied as a boundary condition on the corresponding metacarpal head side to simulate the four laxity tests. The trapezium and second metacarpal bones were fully constrained with zero degrees of freedom. An optimization method was performed to adjust the stiffness of the springs to fit the displacement data measured in the experiment. Optimization was performed using the Levenberg-Marquardt method. A global objective function f_{global} was defined to minimize the square difference between the metacarpal bone displacement in all the simulations and all the experiments, by the summation of the objective function in each simulation f_{flex}, f_{ext}, f_{add}, and f_{abd} as follows:

$$f_{flex} = \sum_{n} \sqrt{\left(\theta(n)_{flex\_exp} - \theta(n)_{flex\_sim}\right)^2} \quad (1)$$

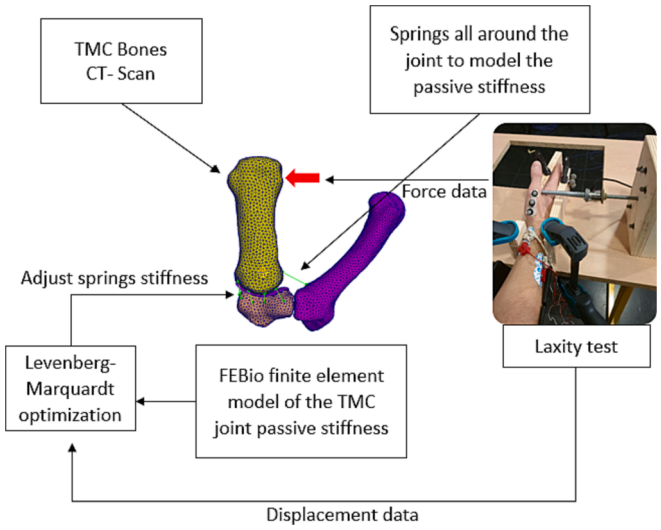

Fig. 2. The optimization process used in this study to optimize the passive stiffness of the TMC joint. This process was performed to create a patient-specific estimation of TMC joint passive stiffness for each participant.

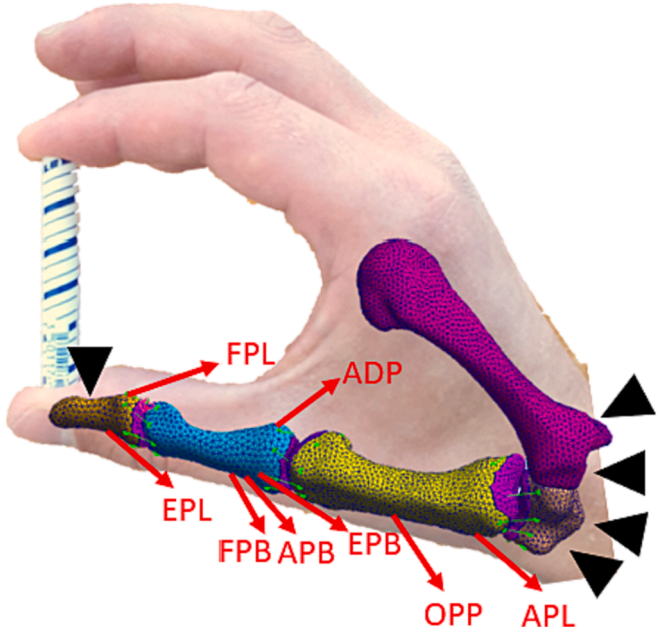

Fig. 3. The finite element model of the thumb joint developed to study the TMC joint stiffness effect on the mechanical loading of the joint during a pinch grip task. The linear springs placed on the joints are represented in green and the muscle forces applied are represented by red arrows. Black triangles represent the degrees of freedom removed for the distal phalanx, the trapezium, and the second metacarpal. This model was run in FEBio. (For interpretation of the references to colour in this figure legend, the reader is referred to the web version of this article.)

$$f_{ext} = \sum_n \sqrt{(\theta(n)_{ext\_exp} - \theta(n)_{ext\_sim})^2} \tag{2}$$

$$f_{add} = \sum_n \sqrt{(\theta(n)_{add\_exp} - \theta(n)_{add\_sim})^2} \tag{3}$$

$$f_{abd} = \sum_n \sqrt{(\theta(n)_{abd\_exp} - \theta(n)_{abd\_sim})^2} \tag{4}$$

$$f_{global} = f_{flex} + f_{ext} + f_{add} + f_{abd} \tag{5}$$

θ(n) is the metacarpal bone rotation angle at each time sample n of the corresponding laxity test (the metacarpal bone flexion angle for the flexion laxity test, and the other corresponding angle for the other tests). Different initial values of linear spring stiffness were tested to find the best initial value to get the best curve fitting (the curve fitting with the minimum value of f_{global}). A custom Python script was developed to implement the Levenberg-Marquardt algorithm and to facilitate interaction between experimental data and the FEBio model. The finite element model was run in FEBio (Maas et al., 2012). The optimization process is summarized in Fig. 2. Stiffness of each participant was then used to simulate the effect of stiffness on the mechanical loading of the TMC joint during a pinch grip task (see next part).

2.3. FE model of the thumb to study the effect of stiffness in pinch grip

To investigate the effect of the TMC joint stiffness on the mechanical loading of cartilage, a pinch grip task was simulated. An entire thumb with the distal and the proximal phalanx was modeled from CT images from the same patient as the optimized model but realized in a pinch grip task (abduction: 14.5°, flexion: 6.6°, rotation: 7.4°, average joint space: 1.5 mm) (Fig. 3). The same process of meshing was performed to model distal and proximal phalanx bones and cartilage. Linear springs were modeled in the metacarpophalangeal and the interphalangeal joints. Their stiffness was set at 100 000 $N.mm^{-1}$ to ensure model stability. The degree of freedom of the thumb distal phalanx in the dorso-palmar plane was removed while the degrees of freedom in the other two planes and around the three axes were unconstrained. Degrees of freedom of the trapezium and second metacarpal bones were fully constrained. We simulated a pinch grip task with an external force of 60 N, modeled by taking the kinematic and force data, recorded during this task, as input of an MBR model to estimate the muscle forces (Goislard de Monsabert et al., 2014). These muscle forces were applied as boundary conditions on the thumb FE model by identifying muscle attachment on bones and muscle force directions (Chao et al., 1989). This task was simulated with the eight spring stiffness configurations of the eight participants (obtained by the experimental evaluation of TMC joint stiffness through the optimization process), to investigate the effect of stiffness on the mechanical loading of cartilage. These simulations were performed to see if the global TMC joint stiffness is negatively correlated with the mechanical loading in terms of joint contact pressure and maximum shear strain. Contact pressure p is defined as the average of the principal stresses σ_{11}, σ_{22}, σ_{33}, and maximum shear strain ε_{shr} is defined as the difference between the maximum and the minimum principal strain ε_{max}, ε_{min} as follows:

$$p = \frac{-(\sigma_{11} + \sigma_{22} + \sigma_{33})}{3} \tag{6}$$

$$\varepsilon_{shr} = \varepsilon_{max} - \varepsilon_{min} \tag{7}$$

These two values were calculated at each node, and then averaged in the joint contact area on the trapezium cartilage surface (where the pressure is different from 0). The global TMC joint stiffness is defined as the sum of the stiffness of each spring for the corresponding participant. These simulations were also run in FEBio (Maas et al., 2012).

Table 1
Results of the optimization performed to optimize each spring stiffness to fit force–displacement data of each participant's laxity test. This table shows the sum of each spring which represents the overall stiffness of the TMC joint (for the correlation test), the absolute angle RMSE, and the normalized angle RMSE.

	Participant							
	P1	P2	P3	P4	P5	P6	P7	P8
Spring stiffness (N/mm)	105.7	121.6	133.9	149.0	122.0	110.9	182.6	132.4
Absolute angle RMSE between experiment and simulation (Radians)	0.021	0.053	0.031	0.021	0.044	0.012	0.018	0.018
Normalized angle RMSE between experiment and simulation (%)	11.3	32.7	16.1	19.0	23.5	14.4	10.1	7.8

Note. The normalized angle RMSE corresponds to the absolute angle RMSE divided by the maximum angle measured during each laxity test and the spring stiffness corresponds to the sum of each individual spring stiffness.

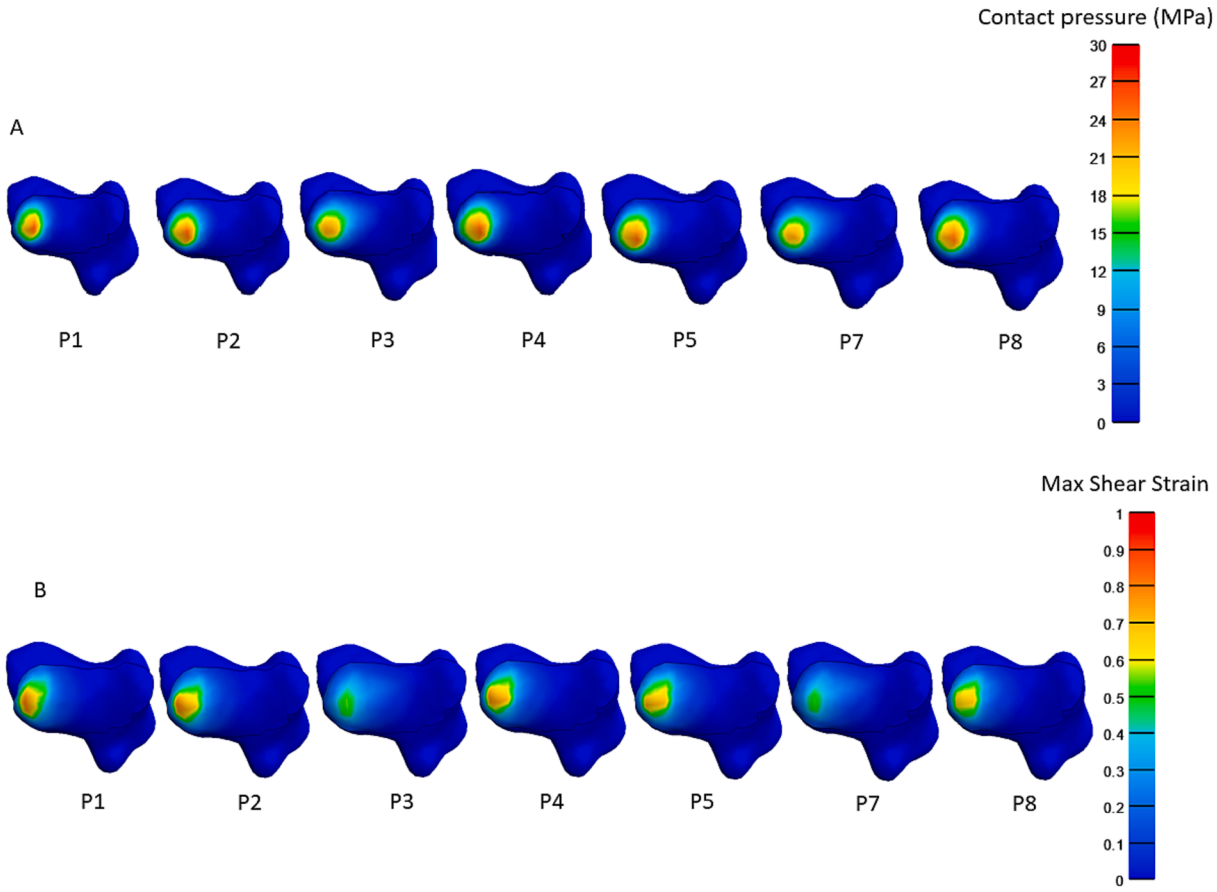

Fig. 4. Distribution plot of the TMC joint contact pressure (A) and maximum shear strain (B) in the trapezium cartilage for each participant. Plot of the participant P6 is not presented due to the unsuccessful simulation. This figure shows the contact pressure and the maximum shear strain at the end of the simulation.

2.4. Statistical analysis

Linear regression analyses were performed, considering TMC joint contact pressure and maximum shear strain as response variables and participant stiffness as explanatory variables. A Pearson test was used to evaluate the significance of the correlation. Data processing and statistical analysis were performed with Python. The Python modules Scipy and Statsmodels were used for statistical analysis. The significance threshold was set at $p < 0.05$.

3. Results

3.1. Spring stiffness determined by the laxity test

The normalized root mean square error (RMSE) between experimental and simulated force–displacement data averaged 16.9 %. The sum of each linear spring stiffness (which defined the global TMC joint stiffness) averaged 132.1 ± 22.9 $N.mm^{-1}$ (range: 105.7 – 182.6 $N.mm^{-1}$). The stiffness for one spring only ranges from 4.9 to 24.7 $N.mm^{-1}$. The stiffness obtained by the optimization and the RMSE for all the participants is presented in Table 1.

Table 2
Results of joint contact pressure and maximum shear strain for each participant. The values reported here correspond to the average values calculated on the joint contact area.

	P1	P2	P3	P4	P5	P7	P8
Joint contact pressure (MPa)	10.0	9.8	8.9	9.8	9.5	8.1	9.4
Maximum shear strain	0.32	0.31	0.22	0.34	0.33	0.22	0.30

3.2. TMC joint contact pressure and maximum shear strain during pinch grip task

TMC joint contact pressure and maximum shear strain distribution

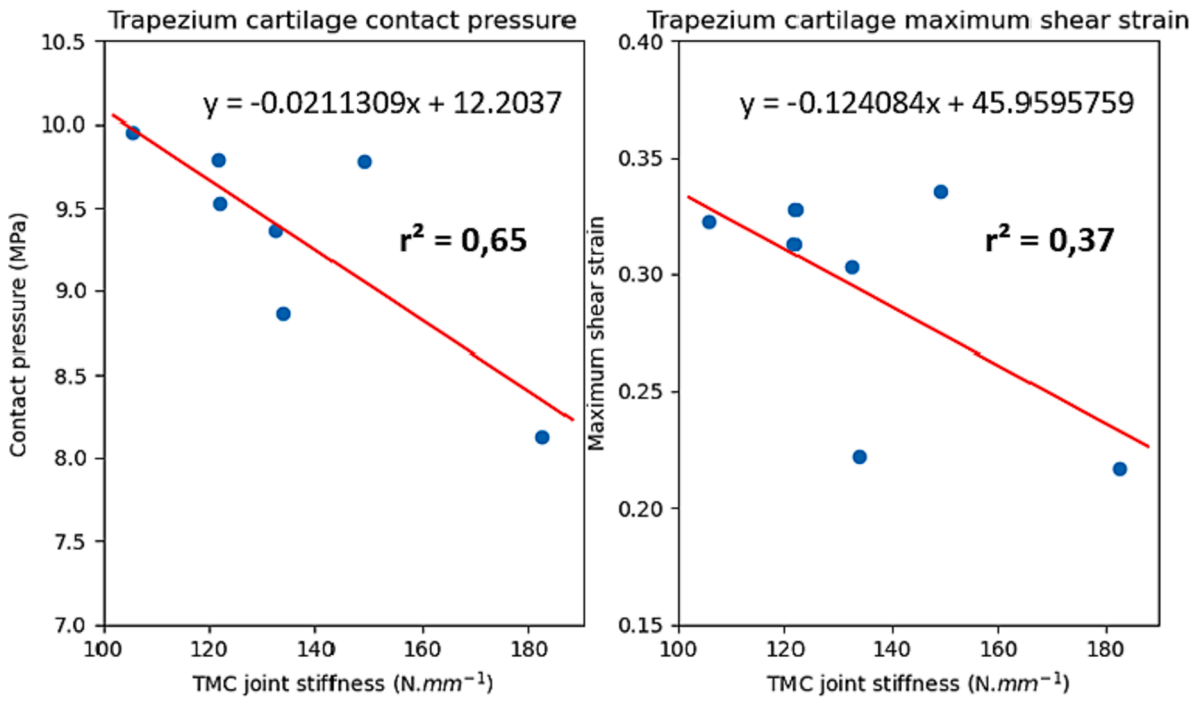

Fig. 5. Linear regression between TMC joint contact pressure, maximum shear strain on cartilage, and TMC joint stiffness of each participant with the successful simulation. The averaged TMC joint contact pressure and maximum shear strain for each participant are represented by blue points and the regression lines by red lines. (For interpretation of the references to colour in this figure legend, the reader is referred to the web version of this article.)

are presented in Fig. 4. Among the eight simulations tested with the stiffness of the eight participants, only seven simulations were completed successfully. For one participant, excessive loading on the cartilage edge during the simulation caused a convergence problem. Results of the TMC joint pressure for this participant (the participant P6) are not presented.

The TMC joint contact pressure and maximum shear strain averaged 9.3 ± 0.6 MPa and 0.29 ± 0.05 respectively. The TMC joint contact pressure and maximum shear strain for each participant are visible in Table 2. The maximal difference in joint contact pressure is observed between participants P1 and P7 with a difference of 23.4 %. The maximal difference in maximum shear strain is observed between participants P4 and P3/P7 with a difference of 54.5 %.

3.3. Correlation between TMC joint stiffness and TMC joint mechanical loadings

Pearson test reveals a significant correlation between TMC joint stiffness and TMC joint contact pressure ($r^2 = 0.65$; $p < 0.05$). No significant correlation was found between the TMC joint stiffness and the TMC joint maximum shear strain ($r^2 = 0.37$; $p > 0.05$). Due to the unsuccessful simulation of participant P6, only seven samples were taken for the two tests. The linear regression plots of the relationship between the TMC joint stiffness and the TMC joint contact pressure and maximum shear strain are presented in Fig. 5.

4. Discussion

The objectives of this study were to propose a method to estimate patient-specific TMC joint passive stiffness and to clarify the effect of TMC joint stiffness on the mechanical loading of the joint and its potential implications for OA risks. To achieve this goal, laxity tests were performed on eight healthy humans to estimate patient-specific joint stiffness by inverse finite element analysis. A finite element model of the entire thumb in a pinch grip task was then used to investigate the effect of stiffness on cartilage contact pressure and maximum shear strain. A linear regression was performed to analyze the correlation between TMC joint stiffness and cartilage contact pressure and maximum shear strain.

The strain values varied significantly between participants with up to 54.5 % inter-individual differences. The maximum cartilage shear strain averages 0.29 for all participants, which is higher than the average values reported by a previous study on the knee (Chan et al., 2016). This previous study reported femoral and tibial cartilage maximum shear strain slightly below 0.1. This important difference could be explained by the mechanical properties used to model the cartilage in this study. The neo-Hookean model could correctly represent the mechanical response of cartilage at the macroscopic level and justify its frequent use in this kind of approach (Dong et al., 2023; Faudot et al., 2020b; Schneider et al., 2017). However, the fluid part of the cartilage is omitted with this approach and could nevertheless influence the stress–strain relationship. A more complex cartilage model should be used in further studies to integrate the tissue complexity and improve the model's accuracy. This more complex approach will also provide some other interesting variables like cartilage fluid velocity, which is one of the best variables for understanding cartilage degeneration according to previous literature (Orozco et al., 2018). Another important parameter to take into account in future studies is also subject-specific cartilage thickness, which can increase contact pressure estimation accuracy, according to the thickness variation observed in previous literature (Dourthe et al., 2019). Nevertheless, we can suppose that, even if the patient-specific cartilage thickness variations can modify the maximal contact pressure, the average contact pressure should be comparable with our results, as was observed for the hip joint (Anderson et al., 2010). It also explains why average pressure was investigated in this study. Beyond modeling questions, our study already suggests a relatively significant inter-individual variation in shear strain on TMC cartilage that needs to be studied in light of a potential risk factor of OA.

The significant correlation found between the TMC joint stiffness, and the joint contact pressure (Fig. 5) confirmed our hypothesis. This correlation could be explained by the metacarpal bone movement increase and the consequences on the cartilage contact. Our results also indicate a possible difference of 23.4 % (the maximal difference

observed in the results) between the higher and lower stiffness. These findings indicate a significant effect of passive stiffness on TMC contact pressures and thus the necessity to individualize it in the FE models. A previous study on the knee joint had shown the same conclusions with a sensitivity analysis performed on a knee FE model (Rooks et al., 2022). Considering cartilage response to high mechanical loadings, this difference of 23.4 % could increase the risk of OA development in the long term (Buckwalter et al., 2013; Eskelinen et al., 2019; Hashimoto et al., 2009; Mononen et al., 2018; Orozco et al., 2018; Saarakkala et al., 2010; Saarakkala and Julkunen, 2010; Turunen et al., 2013; Yin and Xia, 2014).

Nevertheless, some limitations should be considered. Stiffness is not a unique factor that could be correlated with joint contact pressure. An important interindividual variability was also reported on TMC bony morphology (Rusli and Kedgley, 2020) and could also influence joint contact pressure (Schneider et al., 2017). A recent study of our group showed that trapezium dorso-volar curvature is correlated with joint contact pressure during pinch grip tasks (Valerio et al., 2023). In this previous study, joint contact pressure ranges from 6.8 to 15.8 MPa with various morphology against 8.1 to 10.0 MPa with various stiffness in this study. In our study, we consider one bone morphology to analyze the single effect of stiffness. However, further studies should test the combined effect of morphology and stiffness to see how they interact. This study focuses on the stiffness effect on one pinch grip task in one joint position and previous literature has shown that the task can influence pressure distribution in the TMC joint (Schneider et al., 2017). Other TMC joint positions should be tested in the simulations to see the interaction between the stiffness and the posture. The important RMSE values, especially for the participant P2 could be another limitation to the stiffness estimated by the model. The model performance could be improved in future studies by using other techniques like fluoroscopy to improve bone kinematic measurement accuracy (Miura et al., 2004). With this kind of technique, the displacement measured in the four directions could be more accurate and it could be easier to fit the displacement data with the optimization algorithm.

Despite these limitations, this study provided an innovative method to create patient-specific estimations of TMC joint stiffness and highlight the necessity to individualize this parameter in the computational models to ensure good accuracy. Our results indicate a correlation between stiffness and joint contact pressure and can suggest an effect of hypermobility on OA development. Further studies must investigate the stiffness effect in different configurations, with more samples and in interaction with the other parameters to confirm these findings.

CRediT authorship contribution statement

Thomas Valerio: Writing – original draft, Validation, Software, Resources, Methodology, Investigation, Funding acquisition, Formal analysis, Data curation, Conceptualization. **Jean-Louis Milan:** Supervision, Project administration. **Benjamin Goislard de Monsabert:** Supervision, Project administration. **Laurent Vigouroux:** Supervision, Project administration.

Declaration of competing interest

The authors declare that they have no known competing financial interests or personal relationships that could have appeared to influence the work reported in this paper.

References

Anderson, A.E., Ellis, B.J., Maas, S.A., Weiss, J.A., 2010. Effects of idealized joint geometry on finite element predictions of cartilage contact stresses in the hip. J. Biomech. 43, 1351–1357. https://doi.org/10.1016/j.jbiomech.2010.01.010.

Barry, A.J., Murray, W.M., Kamper, D.G., 2018. Development of a dynamic index finger and thumb model to study impairment. J. Biomech. 77, 206–210. https://doi.org/10.1016/j.jbiomech.2018.06.017.

Bettinger, P.C., Smutz, W.P., Linscheid, R.L., Cooney, W.P., An, K.-N., 2000. Material properties of the trapezial and trapeziometacarpal ligaments. J. Hand Surg. 25, 1085–1095. https://doi.org/10.1053/jhsu.2000.18487.

Buckwalter, J.A., Anderson, D.D., Brown, T.D., Tochigi, Y., Martin, J.A., 2013. The roles of mechanical stresses in the pathogenesis of osteoarthritis: Implications for treatment of joint injuries. Cartilage 4, 286–294. https://doi.org/10.1177/1947603513495889.

Chan, D.D., Cai, L., Butz, K.D., Trippel, S.B., Nauman, E.A., Neu, C.P., 2016. In vivo articular cartilage deformation: noninvasive quantification of intratissue strain during joint contact in the human knee. Sci. Rep. 6, 19220. https://doi.org/10.1038/srep19220.

Chao, E.Y.S., An, K.-N., Cooney, W.P., Linscheid, R.L., 1989. Biomechanics of the hand: A basic research study. World Scientific. https://doi.org/10.1142/0321.

Cheze, L., Dumas, R., Comtet, J.J., Rumelhart, C., Fayet, M., 2009. A joint coordinate system proposal for the study of the trapeziometacarpal joint kinematics. Comput. Methods Biomech. Biomed. Engin. 12, 277–282. https://doi.org/10.1080/10255840802459404.

Cooney, W.P., Lucca, M.J., Chao, E.Y., Linscheid, R.L., 1981. The kinesiology of the thumb trapeziometacarpal joint. J. Bone Joint Surg. Am. 63, 1371–1381.

Cvijetić, S., Kurtagić, N., Ozegović, D.D., 2004. Osteoarthritis of the hands in the rural population: a follow-up study. Eur. J. Epidemiol. 19, 687–691. https://doi.org/10.1023/b:ejep.0000036794.40723.8e.

D'Agostino, P., Kerkhof, F.D., Shahabpour, M., Moermans, J.-P., Stockmans, F., Vereecke, E.E., 2014. Comparison of the anatomical dimensions and mechanical properties of the dorsoradial and anterior oblique ligaments of the trapeziometacarpal joint. J. Hand Surg. 39, 1098–1107. https://doi.org/10.1016/j.jhsa.2014.02.025.

Domalain, M., Vigouroux, L., Berton, E., 2010. Determination of passive moment-angle relationships at the trapeziometacarpal joint. J. Biomech. Eng. 132, 071009 https://doi.org/10.1115/1.4001397.

Dong, M., Kerkhof, F., Deleu, G., Vereecke, E., Ladd, A., 2023. Using a finite element model of the thumb to study Trapeziometacarpal joint contact during lateral pinch. Clin. Biomech. 101, 105852 https://doi.org/10.1016/j.clinbiomech.2022.105852.

Dourthe, B., Nickmanesh, R., Wilson, D.R., D'Agostino, P., Patwa, A.N., Grinstaff, M.W., Snyder, B.D., Vereecke, E., 2019. Assessment of healthy trapeziometacarpal cartilage properties using indentation testing and contrast-enhanced computed tomography. Clin. Biomech. 61, 181–189. https://doi.org/10.1016/j.clinbiomech.2018.12.015.

Eskelinen, A.S.A., Mononen, M.E., Venäläinen, M.S., Korhonen, R.K., Tanska, P., 2019. Maximum shear strain-based algorithm can predict proteoglycan loss in damaged articular cartilage. Biomech. Model. Mechanobiol. 18, 753–778. https://doi.org/10.1007/s10237-018-01113-1.

Ewing, J.A., Kaufman, M.K., Hutter, E.E., Granger, J.F., Beal, M.D., Piazza, S.J., Siston, R.A., 2016. Estimating patient-specific soft-tissue properties in a TKA knee: Estimating properties of TKA knees. J. Orthop. Res. 34, 435–443. https://doi.org/10.1002/jor.23032.

Faudot, B., Milan, J.-L., Goislard de Monsabert, B., Le Corroller, T., Vigouroux, L., 2020b. Estimation of joint contact pressure in the index finger using a hybrid finite element musculoskeletal approach. Comput. Methods Biomech. Biomed. Engin. 23, 1225–1235. https://doi.org/10.1080/10255842.2020.1793965.

Faudot, B., Milan, J.-L., Goislard de Monsabert, B., Le Corroller, T., Vigouroux, L., 2020a. Estimation of joint contact pressure in the index finger using a hybrid finite element musculoskeletal approach. Comput. Methods Biomech. Biomed. Engin. 23, 1225–1235. https://doi.org/10.1080/10255842.2020.1793965.

Goislard de Monsabert, B., Vigouroux, L., Bendahan, D., Berton, E., 2014. Quantification of finger joint loadings using musculoskeletal modelling clarifies mechanical risk factors of hand osteoarthritis. Med. Eng. Phys. 36, 177–184. https://doi.org/10.1016/j.medengphy.2013.10.007.

Halilaj, E., Moore, D.C., Patel, T.K., Ladd, A.L., Weiss, A.C., Crisco, J.J., 2015. Early osteoarthritis of the trapeziometacarpal joint is not associated with joint instability during typical isometric loading. J. Orthop. Res. 33, 1639–1645. https://doi.org/10.1002/jor.22936.

Hashimoto, S., Nishiyama, T., Hayashi, S., Fujishiro, T., Takebe, K., Kanzaki, N., Kuroda, R., Kurosaka, M., 2009. Role of p53 in human chondrocyte apoptosis in response to shear strain. Arthritis Rheum. 60, 2340–2349. https://doi.org/10.1002/art.24706.

Jónsson, H., Elíasson, G.J., Jónsson, Á., Eiríksdóttir, G., Sigurðsson, S., Aspelund, T., Harris, T.B., Guðnason, V., 2009. High hand joint mobility is associated with radiological CMC1 osteoarthritis: The AGES-Reykjavik study. Osteoarthritis Cartilage 17, 592–595. https://doi.org/10.1016/j.joca.2008.10.002.

Jonsson, H., Valtysdottir, S.T., Kjartansson, O., Brekkan, A., 1996. Hypermobility associated with osteoarthritis of the thumb base: a clinical and radiological subset of hand osteoarthritis. Ann. Rheum. Dis. 55, 540–543. https://doi.org/10.1136/ard.55.8.540.

Kang, K.-T., Kim, S.-H., Son, J., Lee, Y.H., Chun, H.-J., 2016. Computational model-based probabilistic analysis of in vivo material properties for ligament stiffness using the laxity test and computed tomography. J. Mater. Sci. Mater. Med. 27, 183. https://doi.org/10.1007/s10856-016-5797-z.

Kempson, G.E., 1972. Mechanical properties of articular cartilage. J. Physiol. 223, 23.

Ladd, A.L., Lee, J., Hagert, E., 2012. Macroscopic and microscopic analysis of the thumb carpometacarpal ligaments: A cadaveric study of ligament anatomy and histology. J. Bone Joint Surg. Am. 94, 1468–1477. https://doi.org/10.2106/JBJS.K.00329.

Maas, S.A., Ellis, B.J., Ateshian, G.A., Weiss, J.A., 2012. FEBio: Finite elements for biomechanics. J. Biomech. Eng. 134, 011005 https://doi.org/10.1115/1.4005694.

Marshall, M., Watt, F.E., Vincent, T.L., Dziedzic, K., 2018. Hand osteoarthritis: clinical phenotypes, molecular mechanisms and disease management. Nat. Rev. Rheumatol. 14, 641–656. https://doi.org/10.1038/s41584-018-0095-4.

Miura, T., Ohe, T., Masuko, T., 2004. Comparative in vivo kinematic analysis of normal and osteoarthritic trapeziometacarpal joints. J. Hand Surg. 29, 252–257. https://doi.org/10.1016/j.jhsa.2003.11.002.

Mononen, M.E., Tanska, P., Isaksson, H., Korhonen, R.K., 2018. New algorithm for simulation of proteoglycan loss and collagen degeneration in the knee joint: Data from the osteoarthritis initiative: New algorithm for simulation of proteoglycan loss and collagen degeneration. J. Orthop. Res. 36, 1673–1683. https://doi.org/10.1002/jor.23811.

Moriatis Wolf, J., Turkiewicz, A., Atroshi, I., Englund, M., 2014. Prevalence of doctor-diagnosed thumb carpometacarpal joint osteoarthritis: an analysis of Swedish health care. Arthritis Care Res. 66, 961–965. https://doi.org/10.1002/acr.22250.

Norose, M., Nimura, A., Tsutsumi, M., Fujita, K., Okawa, A., Akita, K., 2022. Anatomical study for elucidating the stabilization mechanism in the trapeziometacarpal joint. Sci. Rep. 12, 20790. https://doi.org/10.1038/s41598-022-25355-3.

Orozco, G.A., Tanska, P., Florea, C., Grodzinsky, A.J., Korhonen, R.K., 2018. A novel mechanobiological model can predict how physiologically relevant dynamic loading causes proteoglycan loss in mechanically injured articular cartilage. Sci. Rep. 8, 15599. https://doi.org/10.1038/s41598-018-33759-3.

Rooks, N.B., Besier, T.F., Schneider, M.T.Y., 2022. A Parameter sensitivity analysis on multiple finite element knee joint models. Front. Bioeng. Biotechnol. 10, 841882 https://doi.org/10.3389/fbioe.2022.841882.

Rusli, W.M.R., Kedgley, A.E., 2020. Statistical shape modelling of the first carpometacarpal joint reveals high variation in morphology. Biomech. Model. Mechanobiol. 19, 1203–1210. https://doi.org/10.1007/s10237-019-01257-8.

Rusli, W.M.R., Mirza, E., Tolerton, S., Yong, S., Johnson, R., Horwitz, M.D., Kedgley, A. E., 2021. Ligamentous constraint of the first carpometacarpal joint. J. Biomech. 128, 110789 https://doi.org/10.1016/j.jbiomech.2021.110789.

Saarakkala, S., Julkunen, P., 2010. Specificity of fourier transform infrared (FTIR) microspectroscopy to estimate depth-wise proteoglycan content in normal and osteoarthritic human articular cartilage. Cartilage 1, 262–269. https://doi.org/10.1177/1947603510368689.

Saarakkala, S., Julkunen, P., Kiviranta, P., Mäkitalo, J., Jurvelin, J.S., Korhonen, R.K., 2010. Depth-wise progression of osteoarthritis in human articular cartilage: investigation of composition, structure and biomechanics. Osteoarthritis Cartilage 18, 73–81. https://doi.org/10.1016/j.joca.2009.08.003.

Schneider, M.T.Y., Zhang, J., Crisco, J.J., Weiss, A.-P.-C., Ladd, A.L., Mithraratne, K., Nielsen, P., Besier, T., 2017. Trapeziometacarpal joint contact varies between men and women during three isometric functional tasks. Med. Eng. Phys. 50, 43–49. https://doi.org/10.1016/j.medengphy.2017.09.002.

Smith, C., Lenhart, R., Kaiser, J., Vignos, M., Thelen, D., 2015. Influence of ligament properties on tibiofemoral mechanics in walking. J. Knee Surg. 29, 099–106. https://doi.org/10.1055/s-0035-1558858.

Sun, T., Wang, J., Suo, M., Liu, X., Huang, H., Zhang, J., Zhang, W., Li, Z., 2023. The digital twin: a potential solution for the personalized diagnosis and treatment of musculoskeletal system diseases. Bioengineering 10, 627. https://doi.org/10.3390/bioengineering10060627.

Turunen, S.M., Han, S.-K., Herzog, W., Korhonen, R.K., 2013. Cell deformation behavior in mechanically loaded rabbit articular cartilage 4 weeks after anterior cruciate ligament transection. Osteoarthritis Cartilage 21, 505–513. https://doi.org/10.1016/j.joca.2012.12.001.

Valerio, T., Vigouroux, L., Goislard de Monsabert, B., De Villeneuve Bargemon, J.-B., Milan, J.-L., 2023. Original article: Relationship between trapeziometacarpal joint morphological parameters and joint contact pressure: A possible factor of osteoarthritis development. J. Biomech., 111573 https://doi.org/10.1016/j.jbiomech.2023.111573.

Westover, L.M., Sinaei, N., Küpper, J.C., Ronsky, J.L., 2016. Quantifying *in vivo* laxity in the anterior cruciate ligament and individual knee joint structures. Comput. Methods Biomech. Biomed. Engin. 19, 1567–1577. https://doi.org/10.1080/10255842.2016.1170122.

Yin, J., Xia, Y., 2014. Proteoglycan concentrations in healthy and diseased articular cartilage by fourier transform infrared imaging and principal component regression. Spectrochim. Acta. A Mol. Biomol. Spectrosc. 133, 825–830. https://doi.org/10.1016/j.saa.2014.05.092.

Zimmerman, B.K., Ateshian, G.A., 2018. A surface-to-surface finite element algorithm for large deformation frictional contact in febio. J. Biomech. Eng. 140, 081013 https://doi.org/10.1115/1.4040497.